DOI: 10.1002/adma.200501224

# High-$\kappa$ Dielectric Nanofilms Fabricated from Titania Nanosheets

By *Minoru Osada*,* *Yasuo Ebina*, *Hiroshi Funakubo*, *Shintaro Yokoyama*, *Takanori Kiguchi*, *Kazunori Takada*, and *Takayoshi Sasaki*

In the semiconductor industry, increasing density requirements continue to motivate the production of microelectronic devices that function reproducibly at ever-smaller dimensions (a trend known as Moore's law).[1] The need for insulating films with nanometer-scale thickness that show good compatibility with semiconductor technology is a critical issue for future device development.[2] As the film thickness scales down to 10 nm, conventional $SiO_2$ gate dielectrics show a poorly insulating character with high leakage currents of $10^{-3}$–$10^{-1}$ A cm$^{-2}$ due to quantum tunneling,[2,3] thereby causing large energy consumption and deteriorated device reliability. Continued device scaling will therefore require substitution of $SiO_2$ with high-dielectric-constant (high-$\kappa$) metal oxide gate dielectrics that afford high capacitance without reliance on film thickness, thus allowing for efficient charge injection and also reducing tunneling leakage currents.

Here, we show that 2D titania ($Ti_{0.87}O_2$) nanosheets function as a high-$\kappa$ nanomaterial.[4] We have successfully fabricated high-$\kappa$ nanofilms by forming multilayer assemblies of titania nanosheets via a layer-by-layer approach through solution-based processes at room temperature. The use of an atomically flat (001) $SrRuO_3$ (SRO) epitaxial film as the bottom electrode enables the fabrication of atomically uniform, highly dense, and void-free nanofilms that retain the superior electrical properties of the titania nanosheets. These films exhibit a reduced leakage current density ($10^{-9}$–$10^{-7}$ A cm$^{-2}$) with a high relative dielectric constant of ~125, even for thicknesses as low as 10 nm. These results, as well as the facile molecular-scale assembly of the nanostructures, suggest that titania nanosheets are attractive candidates for use in nanocomponent insulating high-$\kappa$ dielectric films.

[*] Dr. M. Osada, Dr. Y. Ebina, Dr. K. Takada, Dr. T. Sasaki
Advanced Materials Laboratory
National Institute for Materials Science
1-1, Namiki, Tsukuba, Ibaraki 305-0044 (Japan)
E-mail: osada.minoru@nims.go.jp
Prof. H. Funakubo, S. Yokoyama
Department of Innovative and Engineered Materials
Tokyo Institute of Technology
4259, Nagatsuta, Midori-ku, Yokohama 226-8502 (Japan)
Dr. T. Kiguchi
Center for Advanced Materials Analysis
Tokyo Institute of Technology
2-12-1, O-okayama, Meguro-ku, Tokyo 152-8550 (Japan)
Dr. T. Sasaki
CREST
Japan Science and Technology Agency
4-1-8, Honcho, Kawaguchi-shi, Saitama 332-0012 (Japan)

In the area of high-$\kappa$ dielectrics, there is currently an intense research effort focused on the synthesis and device integration of various oxide materials.[2,3] Current candidates are placed into two categories according to the $\kappa$ value: simple metal oxides with $\kappa = \sim 10$–$20$, such as $Ta_2O_5$,[5] $HfO_2$[6] and $ZrO_2$,[6a] and materials with $\kappa > 100$, such as rutile-type $TiO_2$[7] and (Ba,Sr)$TiO_3$ (BST).[8] In addition to intrinsic properties such as a high dielectric constant and good insulating properties, high-$\kappa$ gate oxides have to fulfill a number of other requirements for device integration:[9] i) they must be chemically stable in contact with the bottom electrodes (Si and/or metals), ii) for optimal performance, they should have an atomically defined interface with the bottom electrodes, without a low-$\kappa$ interfacial layer, and iii) they should have a simple metal oxide system and be accessible through a low temperature (< 600 °C) process. The last aspect is quite important. For BST films,[8] the film-fabrication process requires complex vapor deposition with high-temperature post-annealing (at temperatures > 600 °C), which often causes both a reduction in the polarizability due to non-stoichiometry, as well as degradation of the bottom electrode. Thus, the development of new high-$\kappa$ oxides fulfilling these requirements represents a critical challenge for materials science.

In searching for alternative materials, we have focused on titania ($Ti_{0.87}O_2$) nanosheets,[4] a new class of nanomaterials that represent a modification of nanometer-sized titanium oxide prepared by delaminating layered titanates into their molecular single sheets (Fig. 1a). Compared with rutile and other high-$\kappa$ oxides, titania nanosheets have some unique features: i) they are completely 2D nanomaterials, with a thickness of 0.7 nm, and ii) due to their colloidal and negatively charged character, they can be self-assembled layer-by-layer via a solution-based process to construct ultrathin films.[10] Therefore, the use of titania nanosheets as building blocks for high-$\kappa$ films could provide a potential route to the room-temperature manufacture of high-$\kappa$ devices, eliminating the degradation of the bottom electrode during the annealing process. Here, we report the performance of high-$\kappa$ nanofilms fabricated from titania nanosheets by a solution-based layer-by-layer approach.

Multilayer films of large-sized titania nanosheets (with an average lateral size of 30 μm) have been fabricated by an electrostatic self-assembly technique, using poly(diallyldimethylammonium) (PDDA) as a counter polycation.[11] As the bottom electrode, we use an atomically flat conducting SRO substrate, consisting of a 50 nm thick (001)-oriented epitaxial SRO layer on a (001) $SrTiO_3$ single crystal. The as-de-

   

ADVANCED MATERIALS

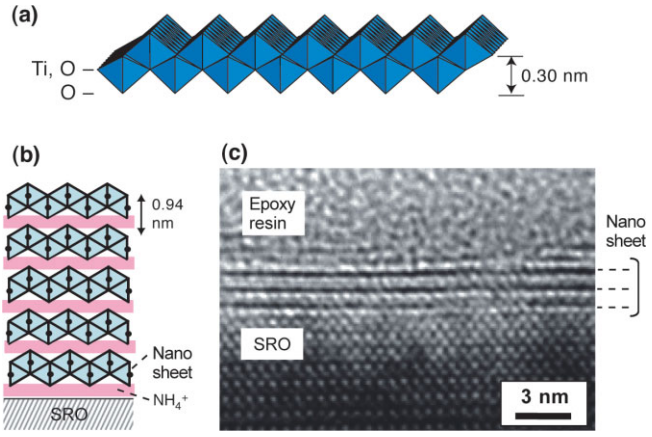


**Figure 1.** High-$\kappa$ dielectric nanofilms composed of titania nanosheets. a) Structure of 2D $Ti_{0.87}O_2$ nanosheets. The Ti atom is coordinated with six oxygen atoms, and the resulting $TiO_6$ octahedra are joined via edge-sharing to produce the 2D lattice. The thickness of the sheets is well below 1 nm, consisting of two edge-shared $TiO_6$ octahedra. b) Structural model for polymer-free multilayer films. c) Cross-sectional high-resolution transmission electron microscopy image of multilayer nanosheets ($n = 5$) on a SRO electrode. Localized chemical analysis by energy-dispersive X-ray spectroscopy from various parts of the sheet-like nanostructures indicates that these nanostructures are composed of Ti and O.

posited $(PDDA/Ti_{0.87}O_2)_n$ films are irradiated with UV light to convert them into a polymer-free form via the photocatalytic activity of the titania nanosheets.[12] In conjunction with previous IR spectroscopy, X-ray diffraction (XRD), and ellipsometry data,[11a] the UV-treated film can be successfully analyzed based on a multilayer-assembly model composed of titania nanosheets and charge-balancing cations such as $NH_4^+$ ions (and/or $H_3O^+$ ions) (Fig. 1b). We have used such polymer-free multilayer films of titania nanosheets $(Ti_{0.87}O_2)_n$ in the following experiments.

Figure 1c shows a cross-sectional high-resolution transmission electron microscopy (HRTEM) image of a multilayer film ($n = 5$) of titania nanosheets. Due to experimental difficulties in preparing cross-sectional specimens, we were unable to observe the entire multilayer structure. Nevertheless, the HRTEM image clearly reveals the stacked structure, corresponding to the layer-by-layer assembly of titania nanosheets. We also note that there is no interfacial layer between $(Ti_{0.87}O_2)_n$ and the SRO electrode. Figure 2 shows atomic force microscopy (AFM) images of monolayer and multilayer films of titania nanosheets. The AFM image of a monolayer film clearly shows the adsorbed nanosheets, which are able to achieve a very efficient (~100 %) coverage of the substrate surface (Fig. 2a) as a consequence of the effective trimming of overlapped patches and crumples by ultrasonication treatment. The film appears flat on the atomic scale and uniform over large areas; the root mean square (rms) roughness is ~0.3 nm. This nearly perfect character persists in the multilayer films (Fig. 2b), which indicates that high-quality monolayers can be repeatedly deposited to yield a well-ordered lamellar structure in multilayer films (Fig. 1b).

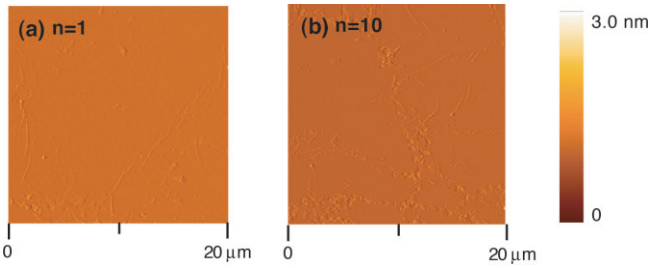


**Figure 2.** AFM images of a) monolayer and b) multilayer nanosheets on SRO electrodes. The root-mean-square roughnesses for the monolayer and multilayer films are 0.31 nm and 0.36 nm, respectively.

The dielectric and leakage current properties of these films have been measured by making $Au/(Ti_{0.87}O_2)_n/SRO$ structures. Figure 3 shows the leakage current density versus voltage ($J$–$V$) curves for multilayer nanosheets with different thicknesses. Here, the thickness of the films has been calibrated using the intersheet spacing (with a periodicity of 0.94 nm) determined from XRD measurements. Our previous study has demonstrated that this can provide a reasonable measure of the thickness value, comparable to values obtained using various characterization techniques including TEM. The $J$ values of these films range from $10^{-9}$–$10^{-7}$ A cm$^{-2}$ (at ±1 V), which are three to five orders-of-magnitude lower than those for rutile $TiO_2$ films (~$10^{-4}$ A cm$^{-2}$) of equivalent thickness.[7b] Moreover, the $J$ level under negative bias (on the top electrode) is always smaller than under positive bias. These $J$ properties are independent of the probe area, showing the good homogeneity of the multilayer films.

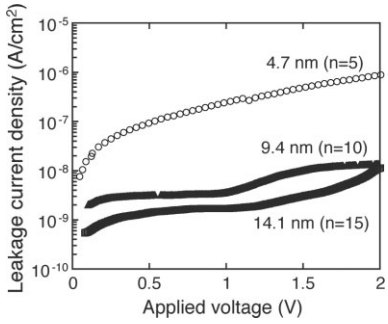


**Figure 3.** Leakage current density versus voltage ($J$–$V$) curves of 4.7 nm ($n = 5$), 9.4 nm ($n = 10$), and 14.1 nm ($n = 15$) thick multilayer nanosheets on SRO electrodes.

Figure 4a shows the variation of the relative dielectric constant $\varepsilon_r$ in the multilayer nanosheets as a function of the film thickness. The $\varepsilon_r$ values of these films are constant around 125, even for thicknesses down to 10 nm. The $\varepsilon_r$ values exhibit a rather flat frequency dispersion (within 5 %) in the $10^3$–$10^7$ Hz regime (not shown here), where the dielectric loss tan$\delta$ is around 2–5 %. We also note that the thickness dependence of the reciprocal capacitance $1/C$ (Fig. 4b) shows a linear rela-

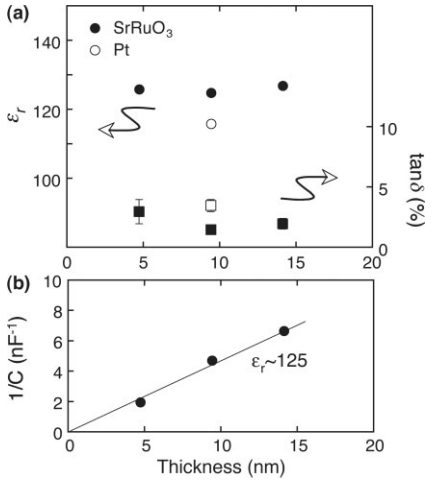


**Figure 4.** a) Variation of the relative dielectric constant $\varepsilon_r$ and the dielectric loss tan$\delta$ in the multilayer nanosheets as a function of the film thickness. Data for 9.4 nm ($n = 10$) thick multilayer nanosheets on Pt electrodes are also included. The dielectric measurements were performed at 10 kHz. b) The thickness dependence of the reciprocal capacitance $1/C$ in multilayer films.

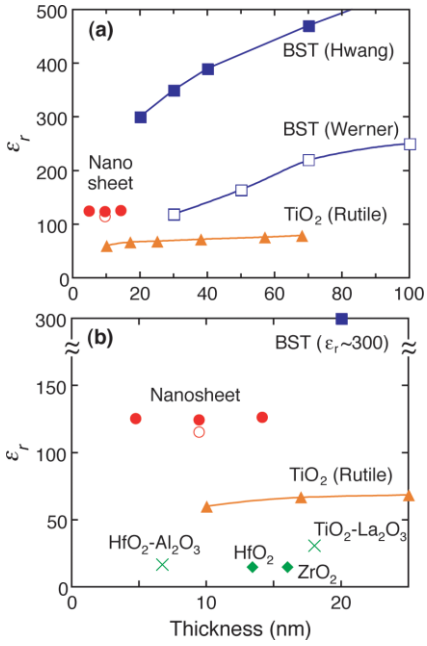


**Figure 5.** a) The maximum values of $\varepsilon_r$ for various high-$\kappa$ materials. b) An expanded view of (a) in the ultrathin region (≤25 nm), including reported data of metal oxides and binary oxide composites [2b,7b,8a,d,e]. For metal oxides such as $HfO_2$ and $ZrO_2$, the dielectric constants do not sharply decrease as the film thickness is reduced to ultrathin dimensions (~10 nm). However, since these materials are usually deposited on Si and experience a rather high-temperature thermal processing that inevitably induces interfacial low-$\kappa$ layer formation, the comparison should be viewed with some caution.

tionship across zero. The estimated value of $\varepsilon_r$ from this $1/C$ slope is ~125, compatible with the measured $\varepsilon_r$ value in Figure 4a. These results indicate the absence of interfacial dead layers inside the films. Thus, the observed high-$\kappa$ properties are material properties inherent to the titania nanosheets.

In Figure 4a we have also included complementary data obtained for Pt/$(Ti_{0.87}O_2)_{10}$/Pt structures. This film shows a slightly smaller $\varepsilon_r$ (~103) compared to a film of the same thickness on a SRO electrode. This is most likely due to the slightly disordered character of the lamellar structure on the Pt electrode. Indeed, the rms roughness (0.8 nm) of the Pt structure is larger than for the SRO case, and this behavior is also compatible with the higher leakage current density ($10^{-6}$ A cm$^{-2}$) of this film. These observations indicate the importance of the atomically flat SRO epitaxial substrate for the construction of a well-ordered lamellar structure with improved $J$ and $\varepsilon_r$ properties.

In Figure 5 we have summarized the maximum $\varepsilon_r$ values for various high-$\kappa$ materials. Figure 5b shows an expanded view of the ultrathin region (≤25 nm), including reported data on metal oxides and binary oxide composites.[2b,7b,8a,d,e] In the ultrathin region (<20 nm), the $\varepsilon_r$ values observed for the multilayer nanosheets are larger than values reported for any other high-$\kappa$ material. We should also emphasize that the high $\varepsilon_r$ value of the multilayer nanosheets persists even in the <10 nm region. This is rather surprising, since in typical high-$\kappa$ materials the dielectric constants have been found to sharply decrease as the film thickness is reduced to ultrathin dimensions (~10 nm); this phenomenon is a long-standing problem in nanometer-scale high-$\kappa$ capacitors. The degradation is more pronounced in materials with larger bulk dielectric constants, as is evident from the comparison between BST and rutile structures (Fig. 5a). In contrast, our results are remarkably different; we observe the simultaneous improvement of $\varepsilon_r$ and the almost total absence of size dependency for the multilayer nanosheets despite the film thickness being in the 10 nm regime.

We now consider the possible origin of the observed high-$\kappa$ properties in titania nanosheets. The high $\varepsilon_r$ value (~125) observed for the multilayer nanosheets can be viewed to be analogous to the bulk properties of the rutile phase. Rutile $TiO_2$ has one of the highest $\kappa$ values (170 along the $c$-axis and 90 along the $a$-axis) among binary metal oxides.[7,13] A recent first-principles study of titania nanosheets and rutile structures revealed that the calculated electronic dielectric constants of single-layer nanosheets are similar to those of rutile.[14] We note that these calculated values are the electronic (high-frequency) contribution, which are different from the static (low-frequency) values measured in this study. This comparison should thus be viewed with some caution. Nevertheless, because of the similar Ti–O bonding character, as well as the larger bandgap of titania nanosheets,[4c] we assume that the titania nanosheets also have a high bulk $\kappa$ value, comparable to rutile.

The $\varepsilon_r$ values (~125) measured for the multilayer nanosheets are excessively high even in ultrathin geometries (~10 nm), which is quite unlike the typical size effects seen for most metal oxides. In typical high-$\kappa$ films, two models have

  

ADVANCED MATERIALS

been used to describe size effects, namely the depoling-field effect and the intrinsic-dead-layer effect. Both of these hypotheses, or versions of them, have been extensively discussed in the literature.[8e] In the depoling-field model, it is assumed that the size effects in high-$\kappa$ films with metal electrodes mainly arise from the electrode interfacial capacitance, which originates from the finite screening length of the polarization-compensating charge distribution of the metal electrode. In the intrinsic-dead-layer model, on the other hand, the dielectric surface inevitably has a certain low-dielectric layer due to the absence of a dielectric material outside the dielectric surface. In our case, the SRO bottom electrode eliminates size effects arising from the depoling field of the electrode, whereas in the absence of detailed information about the Au top electrode, it is not possible to precisely characterize how the interface character of the Au electrode influences the dielectric properties. Nevertheless, the thickness dependence of $1/C$ (Fig. 4b) implies the absence of interfacial dead layers inside the films, and thus the multilayer nanosheets are a rather clean system without strong degradation due to interfacial dead layers and thermal stress. In this context, we note that in preliminary results using other metal electrodes (i.e., Pt/$(Ti_{0.87}O_2)_n$/Pt in Fig. 4a), the $\varepsilon_r$ values are almost the same ($>100$) for a few samples. Thus, even with some intrinsic degradation arising from metal electrodes, additional factors may compensate and/or enhance the dielectric response for multilayer nanosheets in the 10 nm regime.

Experimental observations and theoretical studies suggest that systems with ferroelectric multilayers, superlattices, and nanolaminates exhibit a gigantic dielectric response, similar to the dielectric anomaly near the Curie–Weiss temperature in homogenous ferroelectrics in the vicinity of a critical thickness.[15] In these systems, there is a strong interlayer coupling between the layers that could account for the striking dielectric response properties. We find that this situation is in fact analogous to the structural character of the multilayer nanosheets; each nanosheet is composed entirely of high-$\kappa$ layers and the neighboring layers can form a dipole array, giving rise to some cooperative effects on the dipole state of the neighboring nanosheets. Although theoretical studies of the multilayer nanosheets are required to obtain further understanding of these interlayer-coupling effects, the results presented here should stimulate extensive research on titania nanosheets as possible candidates for nanometer-scale high-$\kappa$ materials.

In summary, we have successfully fabricated high-$\kappa$ nanofilms by forming multilayer assemblies from large-size titania nanosheets. These films show a low leakage current density ($10^{-9}$–$10^{-7}$ A cm$^{-2}$) with a high dielectric constant of ~125 even for thicknesses down to 10 nm. In the ultrathin region (<20 nm), the $\varepsilon_r$ values of the multilayer nanosheets are larger than for any other high-$\kappa$ material. These results clearly suggest that high-$\kappa$ titania nanosheets are model experimental systems for future nanoelectronics technology and fundamental physics, and that soft-chemistry-based fabrication has great potential for the rational design and construction of nanoscale devices. Further interesting possibilities could arise from combining these nanosheets with transparent electronics and molecular devices. This process enables the flexible control of the thickness of ultrathin high-$\kappa$ films in a layer-by-layer fashion. These demonstrated abilities, as well as the absence of costly fabrication steps, provides great advantages that are not attainable using conventional vapor-deposition processes.

## *Experimental*

*Nanosheet and Film Fabrication*: Highly organized multilayer films of large-sized titania nanosheets were fabricated via an electrostatic self-assembly technique followed by ultrasonication treatment. The preparation of titania nanosheets and the fabrication procedure for preparing films have been described in detail previously [11].

The starting layered titanate $K_{0.8}[Ti_{1.73}Li_{0.27}]O_4$ single crystals, grown by a flux method, were converted into a protonic form $H_{1.07}Ti_{1.73}O_4 \cdot H_2O$ in HCl solution. A colloidal suspension of large-sized titania ($Ti_{0.87}O_2$) nanosheets (with an average lateral size of 30 μm) was synthesized by delaminating $H_{1.07}Ti_{1.73}O_4 \cdot H_2O$ with tetrabutylammonium hydroxide solution. An atomically flat conducting SRO substrate, consisting of a 50 nm thick (001) oriented epitaxial SRO film on a (001) $SrTiO_3$ single crystal, was used as the bottom electrode. The SRO substrate (1 cm × 2 cm) was cleaned photochemically with UV light and ozone. The substrate was then pretreated with PDDA ions (20 g dm$^{-3}$, pH 9) for 20 min to introduce a positive charge on the surface. The nanosheets and PDDA were assembled layer-by-layer from a colloidal suspension of the nanosheets (0.08 g dm$^{-3}$, pH 9) and a PDDA solution (20 g dm$^{-3}$, pH 9). The procedure for $Ti_{0.87}O_2$/PDDA deposition was repeated an appropriate number of times to synthesize a multilayer assembly composed of $n$ layer pairs, $(PDDA/Ti_{0.87}O_2)_n$. These films were irradiated with UV light from a Xe lamp (4 mW cm$^{-2}$) for 48 h to convert them into a polymer-free form [12].

*Characterization*: XRD patterns were collected using a Rigaku RINT 2000 powder diffractometer using monochromatized Cu Kα radiation ($\lambda = 0.15405$ nm). HRTEM studies were carried out with a JEOL JEM 3310 microscope operating at 300 kV having a point resolution of 0.17 nm. Cross-sectional TEM specimens were prepared by Ar ion-milling with epoxy glue. A Seiko Instrument SPA-400 AFM was used to examine the topographical features of the film surface.

XRD measurements of as-deposited $(PDDA/Ti_{0.87}O_2)_n$ films showed a Bragg peak (at $2\theta = 5.0°$), which reflects a nanosheet/polycation nanostructure (with a multilayer spacing of 1.5 nm) inside the film. Exposure of the multilayer films to UV light caused a shift of the basal peak to a higher $2\theta$ value, indicating intersheet shrinkage (with a periodicity of 0.94 nm) due to the degradation of the polymer layer via the photocatalytic activity of the titania nanosheets [12]. Previous IR spectroscopy and ellipsometry data revealed that the UV-treated film could be successfully analyzed based on a multilayer-assembly model consisting of titania nanosheets and charge-balancing cations such as $NH_4^+$ ions (and/or $H_3O^+$ ions); this model is quite compatible with the XRD and HRTEM data [12].

*Electrical Measurements*: The electrical measurements were carried out by making Au/$(Ti_{0.87}O_2)_n$/$SrRuO_3$ structures. The 50 nm thick top Au electrode of the capacitor was deposited by vacuum evaporation. The dielectric and leakage current properties were measured using a dielectric test system consisting of an impedance analyzer (HP4194) and a picoammeter (HP4140B), respectively. The dielectric measurements were performed at 10 kHz. Complementary data was also obtained for Pt/$(Ti_{0.87}O_2)_n$/Pt structures.

Received: June 15, 2005
Final version: December 21, 2005

  

[1] G. E. Moore, *Electronics* **1965**, *38*, 114.

[2] a) A. I. Kingon, J.-P. Maria, S. K. Streiffer, *Nature* **2000**, *406*, 1032. b) G. D. Wilk, R. M. Wallace, J. M. Anthony, *J. Appl. Phys.* **2001**, *89*, 5243.

[3] M. Depas, R. L. Van Meirhaegue, W. H. Laflère, F. Cardon, *Solid-State Electron.* **1994**, *37*, 433.

[4] a) T. Sasaki, M. Watanabe, H. Hashizume, H. Yamada, H. Nakazawa, *J. Am. Chem. Soc.* **1996**, *118*, 8329. b) T. Sasaki, M. Watanabe, *J. Am. Chem. Soc.* **1998**, *120*, 4682. c) T. Sasaki, M. Watanabe, *J. Phys. Chem. B* **1997**, *101*, 10 159.

[5] a) P. K. Roy, I. C. Kizilyalli, *Appl. Phys. Lett.* **1998**, *72*, 2835. b) I. C. Kizilyalli, R. Y. S. Huang, P. K. Roy, *IEEE Electron Device Lett.* **1998**, *19*, 341.

[6] a) M. Balog, M. Schieber, S. Patai, M. Michman, *J. Cryst. Growth* **1972**, *17*, 298. b) M. Balog, M. Schieber, M. Michman, S. Patai, *Thin Solid Films* **1997**, *41*, 247. c) H. Zhang, R. Solanki, B. Roberds, G. Bai, I. Banerjee, *J. Appl. Phys.* **2000**, *87*, 1921.

[7] a) M. Kadoshima, M. Hiratani, Y. Shimamoto, K. Torii, H. Miki, S. Kimura, T. Nabatame, *Thin Solid Films* **2003**, *424*, 224. b) S. K. Kim, W.-D. Kim, K.-M. Kim, C. S. Hwang, J. Jeong, *Appl. Phys. Lett.* **2004**, *85*, 4112.

[8] a) C. S. Hwang, S. O. Park, H.-J. Cho, C. S. Kang, H. K. Kang, S. I. Lee, M. Y. Lee, *Appl. Phys. Lett.* **1995**, *67*, 2819. b) C. Basceri, S. K. Streiffer, A. I. Kingon, R. Waser, *J. Appl. Phys.* **1997**, *82*, 2497. c) S. K. Streiffer, C. Basceri, C. B. Parker, S. E. Lash, A. I. Kingon, *J. Appl. Phys.* **1999**, *86*, 4565. d) M. C. Werner, I. Banerjee, P. C. McIntyre, N. Tani, M. Tanimura, *Appl. Phys. Lett.* **2000**, *77*, 1209. e) C. S. Hwang, *J. Appl. Phys.* **2002**, *92*, 432 and references therein.

[9] C. J. Forst, C. R. Ashman, K. Schwarz, P. E. Blochl, *Nature* **2004**, *427*, 53.

[10] T. Sasaki, Y. Ebina, T. Tanaka, M. Harada, M. Watanabe, G. Decher, *Chem. Mater.* **2001**, *13*, 4661.

[11] a) T. Tanaka, K. Fukuda, Y. Ebina, K. Takada, T. Sasaki, *Adv. Mater.* **2004**, *16*, 872. b) T. Tanaka, Y. Ebina, K. Takada, K. Kurashina, T. Sasaki, *Chem. Mater.* **2003**, *15*, 3564.

[12] T. Sasaki, Y. Ebina, K. Fukuda, T. Tanaka, M. Harada, M. Watanabe, *Chem. Mater.* **2002**, *14*, 3524.

[13] U. Diebold, *Surf. Sci. Rep.* **2003**, *48*, 53.

[14] H. Sato, K. Ono, T. Sasaki, A. Yamagishi, *J. Phys. Chem. B* **2003**, *107*, 9824.

[15] a) A. Erbil, Y. Kim, R. A. Gerhardt, *Phys. Rev. Lett.* **1996**, *77*, 1628. b) K. Kukli, J. Ihanus, M. Ritala, M. Leskela, *Appl. Phys. Lett.* **1996**, *68*, 373. c) S. P. Li, J. A. Eastman, J. M. Vetrone, R. E. Newnham, L. E. Cross, *Philos. Mag. B* **1997**, *76*, 47. d) J. Shen, Y. Q. Ma, *Phys. Rev. B: Condens. Matter Mater. Phys.* **2000**, *61*, 14 279. e) A. L. Roytburd, S. Zhong, S. P. Alpay, *Appl. Phys. Lett.* **2005**, *87*, 092 902.


  